NANO LETTERS

Letter

pubs.acs.org/NanoLett

Functional Polyelectrolyte Nanospaced MoS_2 Multilayers for Enhanced Photoluminescence

Piljae Joo,[†,#] Kiyoung Jo,[‡,#] Gwanghyun Ahn,[§] Damien Voiry,[∥] Hu Young Jeong,[⊥] Sunmin Ryu,[§] Manish Chhowalla,*[,∥] and Byeong-Su Kim*[,†]

[†]Department of Chemistry and Department of Energy Engineering, Low Dimensional Carbon Materials Center, Ulsan National Institute of Science and Technology (UNIST), Ulsan 689-798, Korea

[‡]Department of Physics, Ulsan National Institute of Science and Technology (UNIST), Ulsan 689-798, Korea

[§]Department of Chemistry, Pohang University of Science and Technology (POSTECH), Pohang, Gyeongbuk 790-784, Korea

[∥]Materials Science and Engineering, Rutgers University, Piscataway, New Jersey 08854, United States

[⊥]UNIST Central Research Facilities (UCRF), Department of Mechanical and Advanced Materials Engineering, Ulsan National Institute of Science and Technology (UNIST), Ulsan 689-798, Korea

Supporting Information

ABSTRACT: Molybdenum disulfide (MoS_2) multilayers with functional polyelectrolyte nanospacing layers are presented. Taking advantage of the facile method of layer-by-layer (LbL) assembly, individual chemically exfoliated MoS_2 layers are not only effectively isolated from interlayer coupling but also doped by functional polymeric layers. It is clearly demonstrated that MoS_2 nanosheets separated by polymeric trilayers exhibit a much larger increase in photoluminescence (PL) as the number of layers is increased. The enhanced PL has been correlated to the ratio of excitons to trions with the type of polymeric spacers. Because uniform heterogeneous interfaces can be formed between various transition metal dichalcogenides and other soft materials, LbL assembly offers possibilities for further development in the solution-processable assemblies of two-dimensional materials.

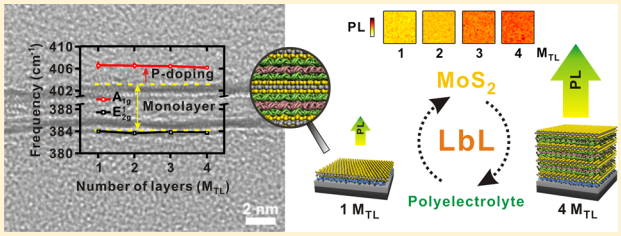

KEYWORDS: *Two-dimensional materials, MoS_2, layer-by-layer assembly, photoluminescence, dopant, exciton*

Since the first successful isolation of graphene, its remarkable properties have renewed interest in other two-dimensional (2D) materials.[1−3] Among them, transition metal dichalcogenides (TMDs) are emerging as a new class of 2D materials with unique mechanical, chemical, electrical, and optical properties.[4−6] Similar to graphene, TMDs can be easily exfoliated into individual monolayers because of the weak van der Waals forces between the layers. The exfoliated 2D crystals of TMDs are direct band gap semiconductors, while their respective bulk counterparts behave as indirect band gap semiconductors. As the thickness decreases, an indirect-to-direct band gap transition of TMDs occurs, accompanied by a band gap increase owing to quantum confinement.[7] For example, molybdenum disulfide (MoS_2), a widely studied TMD, possesses an indirect band gap of 1.3 eV in bulk, which increases to a direct band gap of 1.9 eV in the monolayer form.[8] This indirect-to-direct band gap transition leads to interesting phenomena in MoS_2 monolayers, opening new possibilities for interesting optoelectronic applications.[7] The quantum yield observed so far, however, is significantly smaller than what can be expected from a direct band gap semiconductor; nonetheless, there have been attempts to improve the photoluminescence by placing MoS_2 monolayer on hBN or dielectric substrates, growing large-grained MoS_2 monolayers by CVD, applying strain, gate biasing, covering by oxide, defect engineering, chemical doping, and molecular physisorption.[9−18] These interesting features are based on tuning the exotic electronic band structure of the semiconductor in the 2D limit, and consequently, it is critical to control the number of layers and isolate monolayers for use in potential applications in transistors and optoelectronic devices.

To date, various approaches have been reported to achieve the successful exfoliation into individual (or a few) layers of MoS_2, including micromechanical cleavage, laser or plasma etching, liquid-phase exfoliation assisted by ultrasonication, electrochemical exfoliation, and intercalation-driven exfoliation.[19−23] Morrison and co-workers first reported that Li-intercalation into MoS_2 powders in a solution of *n*-butyllithium results in forced hydration leading to a stable exfoliated suspension of monolayer MoS_2.[23] This solution-processable method is highly desirable for large-scale production and offers a versatile means for the assembly of MoS_2 sheets into films and composites; however, integrating MoS_2 sheets into films over large areas in a simple and reliable manner remains challenging.

Received: August 5, 2014
Revised: September 15, 2014

   dx.doi.org/10.1021/nl502883a | *Nano Lett.* XXXX, XXX, XXX−XXX

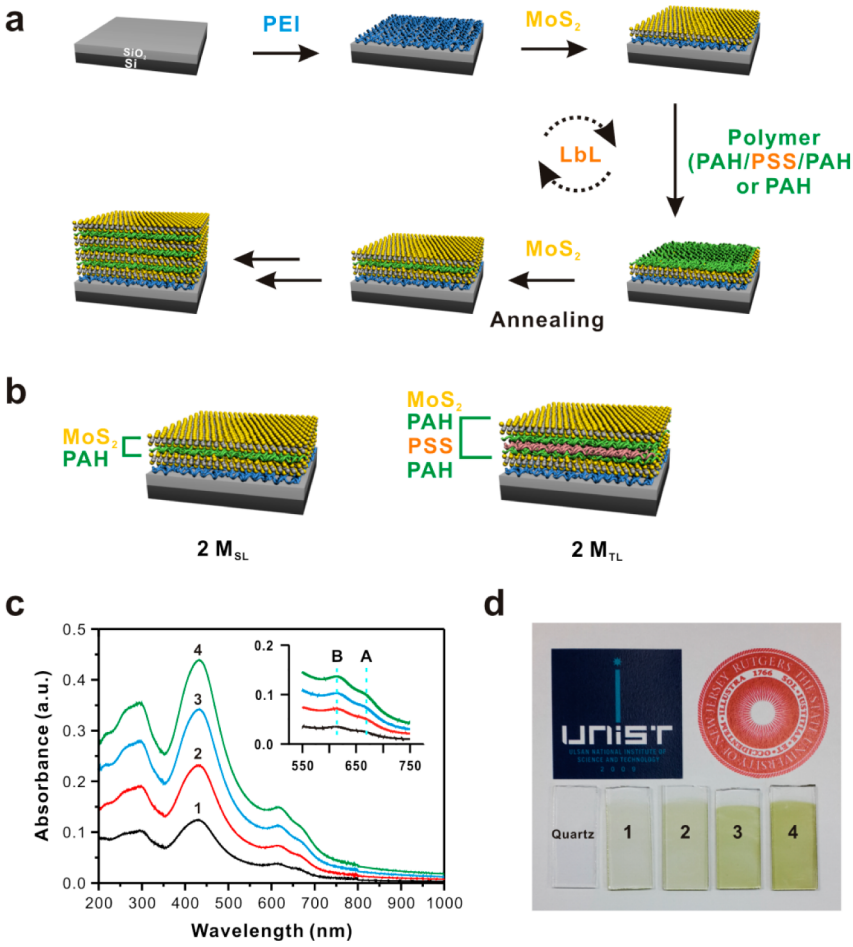

Figure 1. (a) Schematic representation of the LbL assembly of MoS_2 multilayers with regular polymer spacings. See the Supporting Information for details of polymers and assembly conditions. (b) Representation of 2 M_{SL} and 2 M_{TL} multilayers. (c) UV−vis absorbance spectra of the growth of MoS_2 multilayers. The inset shows that excitonic A and B absorbance wavelengths are constant regardless of the increasing numbers of M_{TL} (trilayer polymer spacing). (d) Photograph of MoS_2 multilayer films deposited on a quartz slide with a different number of n M_{TL}.

Here, we demonstrate the first successful fabrication of multilayered MoS_2 films by layer-by-layer (LbL) assembly, showing a significant enhancement of photoluminescence while preserving the innate direct band gap property of MoS_2 sheets through the use of a polymeric spacer. We also found that the polyelectrolyte spacer not only isolates the MoS_2 sheets individually but also induces p-type doping the MoS_2 sheets. The LbL assembly is particularly well-suited for integration of the exfoliated MoS_2 monolayers because it can create highly tunable hybrid thin films with nanoscale control over the composition and structure (e.g., the number of MoS_2 sheets and spacing between the layers). There have been approaches, including our own, to couple unique properties of 2D nanomaterials such as graphene and metal-oxide nanosheets with the versatility of LbL assembly for electronic and biomaterial surfaces; however, many of these studies are limited to creating electrically conducting structures and utilizing them in electronic applications.[24−28]

Results and Discussion. MoS_2 multilayer films were prepared by the sequential LbL assembly between positively charged polymers and negatively charged MoS_2 sheets with a subsequent thermal treatment (Figure 1). The negatively charged MoS_2 suspension was prepared according to a well-known Li intercalation-driven exfoliation method with commercial MoS_2 powder, followed by extensive cycles of centrifugation.[29]

As-prepared MoS_2 suspension exhibited fairly good colloidal stability over a wide range of pH conditions with a ζ-potential of −45 mV because of the adsorption of OH^- on the surface of the MoS_2 sheets.[23] According to the atomic force microscopy (AFM) measurements, the majority of the exfoliated MoS_2 sheets were found to be around 0.50−2.40 μm in the lateral dimension and possessed thicknesses of mono- and a few-layered MoS_2 nanosheets, which was relatively larger than that observed from the mechanically exfoliated MoS_2 monolayers (0.65−0.70 nm) (Supporting Information, Figure S1). With this stable suspension of MoS_2 nanosheets, multilayer thin films of MoS_2 were assembled on a planar silicon wafer or quartz slide by repeatedly layering the suspension of MoS_2 with positively charged polyelectrolytes by electrostatic interaction. In this case, we employed unconventional tetralayer architectures of the LbL assemblies by using four components (one MoS_2 and three polyelectrolyte layers) to ensure a clear separation of MoS_2 layers within the multilayers with an architecture of substrate/PEI/$(MoS_2$/PAH/PSS/PAH$)_{n-1}$/MoS_2 (n = number of MoS_2 layers, typically 1−4) (Figure 1b and see the Supporting Information for experimental details, poly(ethylene imine) (PEI), poly(allylamine hydrochloride) (PAH), and poly(styrenesulfonate) (PSS)). As a control, we

dx.doi.org/10.1021/nl502883a | Nano Lett. XXXX, XXX, XXX−XXX

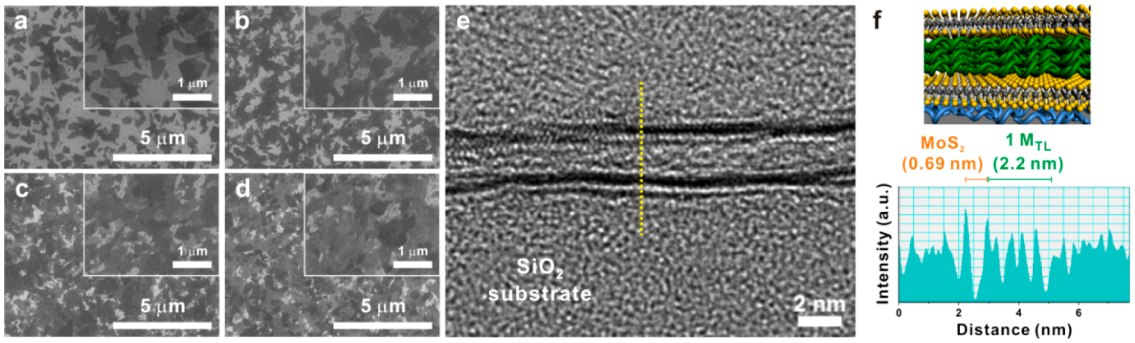

Figure 2. (a–d) SEM images of multilayer MoS_2 films on a SiO_2 substrate with (a) 1 M_{TL}, (b) 2 M_{TL}, (c) 3 M_{TL}, and (d) 4 M_{TL}. The inset shows the corresponding high-magnification image. (e, f) A representative cross-sectional TEM image of 2 M_{TL} MoS_2 multilayer with the corresponding line scan profile representing the thickness of a single MoS_2 nanosheet and single M_{TL} of the MoS_2/polymer.

fabricated the MoS_2 bilayer films using MoS_2 and one polyelectrolyte layer with the architecture substrate/PEI/$(MoS_2/PAH)_{n-1}/MoS_2$ to determine the effect of thickness of the polyelectrolyte layer. Hereafter, we name the samples as n M_{TL} and n M_{SL} for MoS_2 multilayers separated either by a polymeric trilayer (PAH/PSS/PAH; TL) or single-layer (PAH; SL), respectively.

The successful assembly of multilayer MoS_2 films was monitored with a gradual increase in absorbance upon increasing the number of layers in each set of M_{SL} and M_{TL} (Figure 1c,d and Figure S2 in the Supporting Information). The characteristic peaks of MoS_2 between 600 and 700 nm are observed from decoupled valence band due to the spin–orbit coupling at the K point of the Brillouin zone, as similarly demonstrated in previous studies.[29,30] It is of note that the as-assembled MoS_2 multilayers without any thermal treatment did not exhibit the characteristic excitonic peaks, suggesting the successful restoration of the thermodynamically stable trigonal prismatic phase (2H-MoS_2) from the metastable Li-intercalated octahedral 1T-MoS_2 form.[31] Consistent with the absorbance spectra, ellipsometry measurements showed that the thickness of the multilayer MoS_2 films was linearly proportional to the number of M_{TL} with an average M_{TL} thickness of 2.58 nm, suggesting the successful deposition of MoS_2 multilayers (see the Supporting Information, Figure S3).

The surface morphology of multilayer MoS_2 films was observed by scanning electron microscopy (SEM) (Figure 2 and see Figure S4 and S5 in the Supporting Information). Initial MoS_2 layer deposition in 1 M_{TL} did not fully cover the surface because of electrostatic repulsion among the sheets, as often observed in the initial few layers of polyelectrolyte-based LbL systems. As the deposition of MoS_2 progressed, the surfaces were well-covered with thin layers of MoS_2, although some vacant sites were still observed in the SEM images. It should be noted that a few layered flakes were observed in some images owing to difficulties in purifying MoS_2 monolayers by solution processing. Thus, we find that some MoS_2 sheets overlapped with one another on the densely packed surface, which might interrupt the generation of effective photoluminescence. The cross-sectional transmission electron microscopy (TEM) image further revealed the internal structure of the MoS_2 multilayer (Figure 2e and f). Although the initial MoS_2 sheets are not completely isolated as monolayers, we clearly observe the interlayer separation of MoS_2 sheets by the polyelectrolyte spacer. The thickness of 1 M_{TL} in the MoS_2 multilayer corresponds to about 2.2 nm, similar to that collected by ellipsometry.

X-ray photoelectron spectroscopy (XPS) was performed to investigate the composition of the MoS_2 multilayer and influence of thermal annealing at 300 °C under an Ar atmosphere. Figure S6 shows the high-resolution XPS spectra of the representative 1 M_{TL} MoS_2 film. Deconvoluted Mo 3d spectra exhibited two peaks at 229.7 and 232.8 eV that correspond to the Mo^{4+} $3d_{5/2}$ and $3d_{3/2}$ components of the thermodynamically stable 2H-MoS_2, respectively. Similarly, in the S spectrum, additional peaks were found along with the known doublet peaks of 2H-MoS_2 corresponding to S $2p_{3/2}$ and $2p_{1/2}$, which appeared at 162.5 eV and 163.8 eV, respectively. These results indicate the successful transformation of the metastable 1T-MoS_2 form into stable 2H-MoS_2 upon thermal treatment after the assembly, which is in good agreement with previous reports. Additionally, sulfur does not display any signs of further oxidation, which might appear between 168 and 170 eV.

Raman spectroscopy is the most direct and nondestructive technique to confirm the layered structure of MoS_2. Recent studies indicate that the position of the two prominent in-plane E^1_{2g} and out-of-plane A_{1g} peaks are highly dependent on the number of layers of MoS_2.[32,33] For example, the mechanically exfoliated MoS_2 showed a shift in the E^1_{2g} peak from 382 to 384 cm^{-1}, while A_{1g} peak shifted from 407 to 403 cm^{-1} from bulk to monolayer MoS_2, respectively. Accordingly, the evolution of Raman spectra is presented in Figure 3 as a function of the number of MoS_2 layers. Interestingly, we observed that the Raman intensity normalized against the silicon substrate increased linearly as the number of MoS_2 layers increased without noticeable peak shifts of either E^1_{2g} or A_{1g} at 383.6 cm^{-1} and 406.5 cm^{-1}, respectively. The constant interpeak separation (~21 cm^{-1}) is in stark contrast to other reports that observed shifts in the position of both peaks as well as the broadening of the interpeak separation along with the number of layers, clearly indicating the weak interlayer coupling between MoS_2 layers with the aid of polymeric nanospacings.[32,33] In addition, the constant peak separations of MoS_2 multilayers are relatively larger than that observed in monolayer MoS_2 (~19 cm^{-1}).[32] Interestingly, we noticed that the A_{1g} peak exhibits a blue-shift by ~4 cm^{-1} while the E^1_{2g} peak remains constant compared to the pristine MoS_2 monolayer. This is in accordance with previous reports that the A_{1g} mode is highly influenced by carrier concentration. This influence results from the symmetrical vibration of A_{1g}, which can be easily changed by the perturbation of the electrons in the bottom of the conduction band at the K point, while the E^1_{2g} mode is independent of electron–phonon interactions.[34,35]

dx.doi.org/10.1021/nl502883a | Nano Lett. XXXX, XXX, XXX–XXX

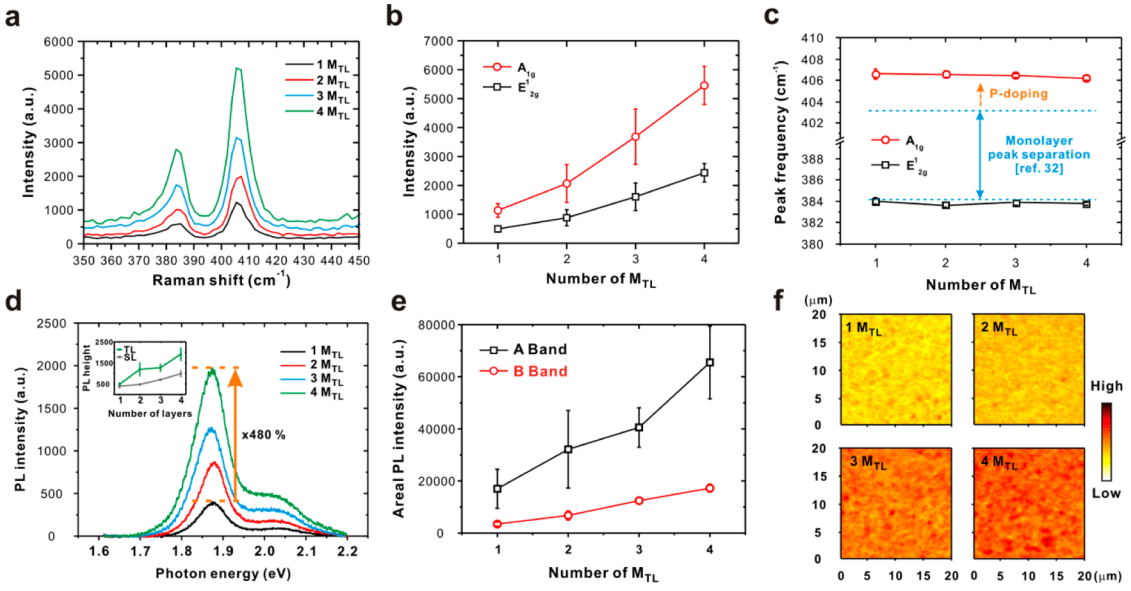

Figure 3. (a) Raman spectra of multilayer MoS_2 films with different numbers of M_{TL}. (b, c) Intensity and peak frequency of A_{1g} and E^1_{2g} peaks with different numbers of M_{TL}. The dotted blue line in (c) represents the peak frequency separation (19 cm^{-1}) of the MoS_2 monolayer. (d, e) Photoluminescence spectra and areal intensities of two peaks from the multilayer MoS_2 films. The inset of (d) is a comparison of photoluminescence intensity between M_{TL} and M_{SL} at the wavelength corresponding to maximum intensity. (f) Photoluminescence intensity mapping of M_{TL} set (20 × 20 μm^2) with a different number of MoS_2 layers. All mappings were conducted with 0.35 mW, 532 nm laser for a 0.01 s integration time in Raman spectroscopy. Signals are obtained from 1.7 to 2.1 eV for each data.

Therefore, the shift in the A_{1g} peak suggests the evidence of p-doping effects brought about by the adjacent polymeric spacing of MoS_2 layers. Further analysis of doping effects on photoluminescence enhancement is described below.

Furthermore, the photoluminescence properties of MoS_2 thin films, arising from the isolated direct band gap of monolayer MoS_2 sheets, are evaluated. The photoluminescence spectra were collected with a Raman instrument at excitation wavelength of 514 nm and normalized against the silicon substrate peak.[36,37] According to a recent study by Eda and co-workers, thin monolayers of MoS_2 prepared by Li-intercalation of MoS_2 exhibits the strongest photoluminescence, while the emission intensity gradually decreases with increasing film thickness.[29] Interestingly, however, we found that the normalized photoluminescence intensity of the LbL-assembled MoS_2 films gradually increased as the number of M_{TL} increased in a large area uniformity (20 × 20 μm^2), with a major emission peak appearing around 659 nm and a minor peak at 605 nm (Figure 3d, e, and f). Specifically, we compared the maximum photoluminescence intensities of 1−4 M_{TL}'s to investigate how each polymeric layer screens the interlayer coupling of MoS_2 layers. The maximum peak intensity for each photoluminescence spectrum was chosen to directly compare the contribution of only the major peak enhancement, which corresponds to a band gap of 1.9 eV. Interestingly, photoluminescence increased by approximately 480%, while the M_{SL} set exhibited only a 347% increase (Figure 3d and Figure S7 in the Supporting Information). To determine why such a difference was observed, we extrapolated that the enhanced photoluminescence was originated from the effective isolation of individual MoS_2 sheets because there was no obvious red-shift of the MoS_2 exciton absorption peak as previously reported (inset in Figure 1b).[29,38] This postulation is clearly evident because the M_{SL} set, which is separated by thinner isolating layers, exhibits slight shift of excitonic absorbance peak and a lower photoluminescence than that of M_{TL} due to interlayer coupling (see the Supporting Information, Figure S1, and inset of Figure 3d). This is consistent with the fact that the photoluminescence increase of the M_{SL} set is less than 400%, which means that each monolayer does not work independently. Furthermore, photoluminescence quantum yield (QY) measurements which were calibrated by rhodamine 6G verified the effective isolation of each MoS_2 layers within multilayers (see the Supporting Information, Figure S8). Interestingly, M_{TL} set maintained nearly constant QY values of ~1.2 × 10^{-3} along whole number of layers which are comparable to the previous result of monolayer MoS_2 (4 × 10^{-3}), while M_{SL} displayed degradation as the number of layer increases.[7] The areal photoluminescence intensity, in fact, increases by less than 480%, even in the M_{TL} set. We suspect that this tendency originates from nature of chemical exfoliation process generating some defects, which can act as scattering centers and cause deviations in the energy of the emitted photons. To investigate defect-assisted broadening of photoluminescence peaks, we compared the full-width-at-half-maximum (fwhm) values of samples (see the Supporting Information, Figure S9). The values of A peak from 1−4 M_{TL} samples are located in a range of 70−90 meV, comparable to previously reported value of 90 meV extracted from exfoliated MoS_2 monolayer on SiO_2 by scotch-tape method.[18]

To investigate the origin of layer-dependent additional enhancement of photoluminescence in detail, in particular, 480% improvement of 4 M_{TL} compared to 1 M_{TL} as an example, we consider the exotic 2D excitonic effect in MoS_2. In the highly thin 2D regime, especially in MoS_2, excitons (A^o) and trions (we focus on the negatively charged trion, A^-, because MoS_2 is an n-type semiconductor) derived from strong coulomb interactions significantly contribute to the generation of photoluminescence, even at room temperature, whereas the contribution of trions is negligible in common bulk materials such as GaAs due to its small binding energy.[13,17,39] Recently, it has been reported that a gate bias or chemical doping can

dx.doi.org/10.1021/nl502883a | Nano Lett. XXXX, XXX, XXX−XXX

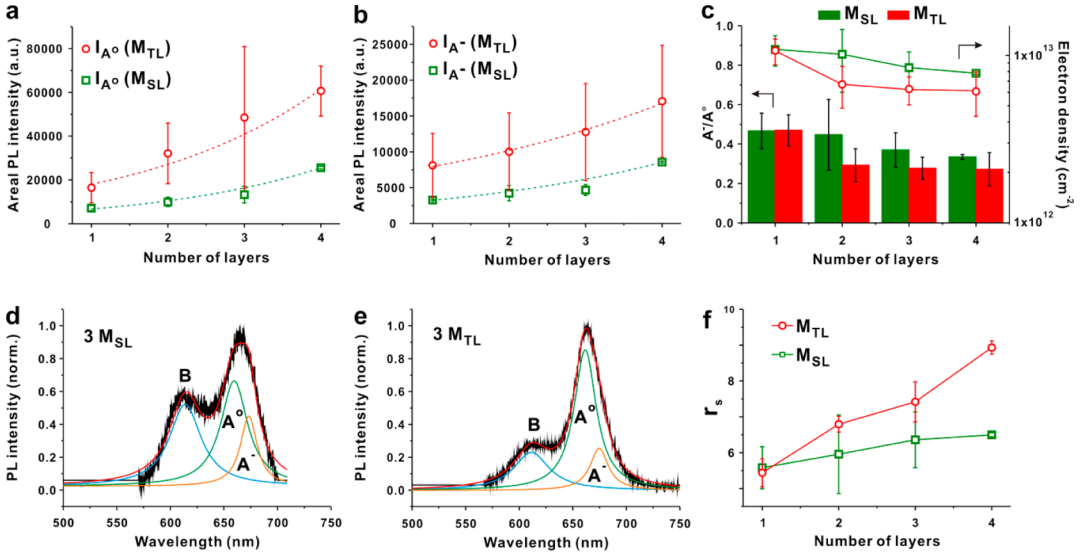

Figure 4. (a, b) Areal photoluminescence intensity of MoS_2 multilayers contributed from exciton and trion, respectively. Dotted lines are the curves fitted by an exponential function. (c) Ratios of trions and excitons for each layer and the corresponding electron density. (d, e) Intensity normalized photoluminescence spectrum of the M_{SL} and M_{TL} sets, respectively. (f) Dimensionless interparticle distance in the M_{SL} and M_{TL} sets.

provide an efficient means for tuning the number of excitons and the corresponding photoluminescence of the MoS_2 monolayer.[13,17,18,40] Therefore, we investigate the contribution of excitonic effects to the photoluminescence of nanospaced MoS_2 multilayers. By comparing the M_{SL} and M_{TL} sets, we find that polyelectrolyte-induced doping effects of the spacing layer are critical in enhancing the photoluminescence. By considering the excitonic peak of A^o (~1.88 eV, 660 nm) and A^- (~1.84 eV, 674 nm), the major A peak of the photoluminescence spectrum of the M_{SL} and M_{TL} sets can be deconvoluted (Figure 4d and e). Accordingly, the M_{SL} and M_{TL} sets display significant differences in the ratio of A^o and A^- (Figure 4c). The M_{SL} set has a relatively high A^- portion compared to that of the M_{TL} set. Furthermore, as the number of layers is increased, the A^- portion in the M_{SL} set is slightly reduced, while the M_{TL} set shows drastic decrease in the ratio. In that regard, because the number of neutral excitons is lower in M_{SL}, the actual contribution of A^- on photoluminescence is relatively small (Figure 4b). This layer-dependent phenomenon demonstrates that each of the MoS_2 layers is effectively doped by the polyelectrolyte nanospacing layer. The corresponding electron density of each of the sets are extracted by the trion spectral weight and mass action law (Figure 4c and see the Supporting Information).[13] For this model, we use the areal photoluminescence intensity to consider the whole number of emitted photons from the MoS_2 layer despite the defect-assisted photoluminescence variation. The result exhibits that electron density gradually decreased upon p-doping as the number of layers increased. The corresponding areal photoluminescence intensity proves that the contribution of excitons on photoluminescence is more than that of trions. The result is very similar to previous photoluminescence tuning results by means of gate-biased monolayer MoS_2 FET and highly doped by other chemicals.[13,17] Among the two different nanospacers, TL (PAH/PSS/PAH) displays a higher electron-withdrawing effect than SL (PAH). The reason is that TL set contains a higher amount of electron-withdrawing groups originated from PAH and PSS than the SL set. Although PSS is a well-known p-dopant, however, the contribution of PSS on doping process is not crucial in this case since it is not directly adjacent to MoS_2, which is in good agreement with the observation of negligible A_{1g} shift compared to that of SL set (see the Supporting Information, Figure S10).[41] The result is also consistent to the systematic emission peak shift of MoS_2 multilayers (see the Supporting Information, Figure S11). Overall, the M_{TL} set shows a higher value than that of the M_{SL} set, meaning that the TL spacer p-dopes MoS_2 more effectively. The layer dependency is quite different between M_{TL} and M_{SL} sets. The M_{TL} set displays nearly constant values because polymeric layers withdraw electrons from only adjacent MoS_2 layers. Thus, degree of doping on MoS_2 becomes constant for each layer within the M_{TL} set (~1 meV). On the other hand, because PL enhancement of M_{SL} is limited by interlayer coupling, a relatively high dependency on the doping process is observed as shown from a gradual A band peak shift (~8 meV).

Moreover, to clearly demonstrate the contribution of both the thickness and doping of each polymeric layer, we elucidate the effect of the polymeric nanospacing layer by extracting the average interparticle distance r_s in the units of the effective Bohr radius, which can be interpreted as a ratio between the Coulomb potential energy and kinetic energy.[13]

$$r_s = \frac{g_v}{\sqrt{\pi n}\,(\epsilon\hbar^2/m_e e^2)}$$

where ϵ is the dielectric constant ($\epsilon = \sqrt{(\epsilon_\parallel \epsilon_\perp)}$; $\epsilon_\parallel = 2.5$, $\epsilon_\perp = 6.76$), m_e is the effective mass of an electron ($m_e = 0.35 m_o$), g_v is the valley degeneracy ($g_v = 2$), and n is the electron density.[13] Due to the high confinement in the ideal 2D system, the r_s values increase as its 2D electron gas approaches that of an ideal system.[42] In our system, the M_{TL} set shows a higher r_s value and an increasing rate compared with the M_{SL} set, and therefore, we conclude that TL is a more efficient spacing layer for realizing a 2D system by controlling the number of excitons in the 2D system, even in the multilayers of MoS_2.

Despite possible structural defects and stacking disorders that might reduce the intensity of the photoluminescence of MoS_2 multilayers, our system is applicable to multilayered MoS_2 structures with relevant nanospacings as supported in recent studies that photoluminescence exists in few-layered MoS_2.[43]

dx.doi.org/10.1021/nl502883a | Nano Lett. XXXX, XXX, XXX−XXX

We have also extended the current approach of assembling 2D nanosheets to include heterocombination with the TMD-like WS_2 system by taking advantage of the LbL method (see the Supporting Information, Figure S12). In fact, photoluminescence of WS_2 was not exhibited because its ambipolar nature diminishes neutral exciton by p-doping of polymeric layer but dual doping process on MoS_2 and WS_2 is out of scope of this paper. It is expected that such combinational versatility will be useful in future work by employing a broad range of material combinations. Furthermore, regarding on the doping of MoS_2, this study is the first report of using polyelectrolyte as an air-stable and solution-processable dopant for TMDs as far as we know (see Table S1 in the Supporting Information). Therefore, our observations suggest that the LbL assembly successfully isolates individual MoS_2 layers with precise nanospacing by incorporating functional polyelectrolyte interlayers that can be used for advanced optoelectronic applications.

Conclusion. In conclusion, we have fabricated MoS_2 multilayers by employing the LbL assembly, which allows for the incorporation of polymeric spacings between individual MoS_2 layers to minimize interlayer coupling. We found that the photoluminescence of LbL-assembled MoS_2 multilayers significantly improved along with the p-doping behavior without altering other properties of the MoS_2 nanosheets. Moreover, heterostructured 2D TMDs were successfully fabricated by LbL assembly. Considering the versatile nature of the LbL assembly coupled with the extraordinary electronic properties of 2D TMDs, we envision that this study will offer opportunities and insights into further development of solution-processable hybrid 2D TMD-based optoelectronic and energy devices.

■ ASSOCIATED CONTENT

Supporting Information

Experimental and additional characterizations by AFM, UV−vis spectra, ellipsometry, SEM, XPS, photoluminescence spectra of the M_{SL} set, quantum yield, fwhm plot, Raman shift of MoS_2 with polymeric layers, A peak photon energy shift, Raman spectrum of the multilayers combined with heterogeneous TMDs, table regarding previous literature about MoS_2 doping effect, and physical description of the exciton−trion equilibrium state. This material is available free of charge via the Internet at http://pubs.acs.org.

■ AUTHOR INFORMATION

Corresponding Authors

*E-mail: bskim19@unist.ac.kr.
*E-mail: manish1@rci.rutgers.edu.

Author Contributions

#P.J. and K.J. contributed equally to this work.

Notes

The authors declare no competing financial interest.

■ ACKNOWLEDGMENTS

This work was supported by the National Research Foundation of Korea (NRF) grant funded by the Korean government (2012R1A1A2040782, 2012-053500). K. Jo acknowledges the financial support from Global Ph.D. Fellowship funded by National Research Foundation of Korea (NRF-2013H1A2A1033123).

■ REFERENCES

(1) Novoselov, K. S.; Jiang, D.; Schedin, F.; Booth, T. J.; Khotkevich, V. V.; Morozov, S. V.; Geim, A. K. *Proc. Natl. Acad. Sci. U.S.A.* **2005**, *102*, 10451.
(2) Wang, Q. H.; Kalantar-Zadeh, K.; Kis, A.; Coleman, J. N.; Strano, M. S. *Nat. Nanotechnol.* **2012**, *7*, 699.
(3) Jariwala, D.; Sangwan, V. K.; Lauhon, L. J.; Marks, T. J.; Hersam, M. C. *ACS Nano* **2014**, *8*, 1102.
(4) Chhowalla, M.; Shin, H. S.; Eda, G.; Li, L. J.; Loh, K. P.; Zhang, H. *Nat. Chem.* **2013**, *5*, 263.
(5) Huang, X.; Zeng, Z. Y.; Zhang, H. *Chem. Soc. Rev.* **2013**, *42*, 1934.
(6) Xu, M.; Liang, T.; Shi, M.; Chen, H. *Chem. Rev.* **2013**, *113*, 3766.
(7) Mak, K. F.; Lee, C.; Hone, J.; Shan, J.; Heinz, T. F. *Phys. Rev. Lett.* **2010**, *105*, 136805.
(8) Li, T. S.; Galli, G. L. *J. Phys. Chem. C* **2007**, *111*, 16192.
(9) Mak, K. F.; He, K.; Shan, J.; Heinz, T. F. *Nat. Nanotechnol.* **2012**, *7*, 494.
(10) Sercombe, D.; Schwarz, S.; Pozo-Zamudio, O. D.; Liu, F.; Robinson, B. J.; Chekhovich, E. A.; Tartakovskii, I. I.; Kolosov, O.; Tartakovskii, A. I. *Sci. Rep.* **2013**, *3*, 3489.
(11) Zhang, W.; Huang, J.-K.; Chen, C.-H.; Chang, Y.-H.; Cheng, Y.-J.; Li, L.-J. *Adv. Mater.* **2013**, *25*, 3456.
(12) Hui, Y. Y.; Liu, X.; Jie, W.; Chan, N. Y.; Hao, J.; Hsu, Y.-T.; Li, L.-J.; Guo, W.; Lau, S. P. *ACS Nano* **2013**, *7*, 7126.
(13) Mak, K. F.; He, K.; Lee, C.; Lee, G. H.; Hone, J.; Heinz, T. F.; Shan, J. *Nat. Mater.* **2013**, *12*, 207.
(14) Li, Z.; Chang, S.-W.; Chen, C.-C.; Cronin, S. *Nano Res.* **2014**, *7*, 973.
(15) Plechinger, G.; Schrettenbrunner, F. X.; Eroms, J.; Weiss, D.; Schüller, C.; Korn, T. *Phys. Status Solidi Rapid Res. Lett.* **2012**, *6*, 126.
(16) Tongay, S.; Suh, J.; Ataca, C.; Fan, W.; Luce, A.; Kang, J. S.; Liu, J.; Ko, C.; Raghunathanan, R.; Zhou, J.; Ogletree, F.; Li, J.; Grossman, J. C.; Wu, J. *Sci. Rep.* **2013**, *3*, 2657.
(17) Mouri, S.; Miyauchi, Y.; Matsuda, K. *Nano Lett.* **2013**, *13*, 5944.
(18) Tongay, S.; Zhou, J.; Ataca, C.; Liu, J.; Kang, J. S.; Matthews, T. S.; You, L.; Li, J.; Grossman, J. C.; Wu, J. *Nano Lett.* **2013**, *13*, 2831.
(19) Castellanos-Gomez, A.; Barkelid, M.; Goossens, A. M.; Calado, V. E.; van der Zant, H. S. J.; Steele, G. A. *Nano Lett.* **2012**, *12*, 3187.
(20) Liu, Y.; Nan, H.; Wu, X.; Pan, W.; Wang, W.; Bai, J.; Zhao, W.; Sun, L.; Wang, X.; Ni, Z. *ACS Nano* **2013**, *7*, 4202.
(21) Coleman, J. N.; Lotya, M.; O'Neill, A.; Bergin, S. D.; King, P. J.; Khan, U.; Young, K.; Gaucher, A.; De, S.; Smith, R. J. *Science* **2011**, *331*, 568.
(22) Zeng, Z.; Yin, Z.; Huang, X.; Li, H.; He, Q.; Lu, G.; Boey, F.; Zhang, H. *Angew. Chem., Int. Ed.* **2011**, *50*, 11093.
(23) Joensen, P.; Frindt, R.; Morrison, S. R. *Mater. Res. Bull.* **1986**, *21*, 457.
(24) Osada, M.; Sasaki, T. *Adv. Mater.* **2012**, *24*, 210.
(25) Hong, J.; Char, K.; Kim, B.-S. *J. Phys. Chem. Lett.* **2010**, *1*, 3442.
(26) Hong, J.; Han, J. Y.; Yoon, H.; Joo, P.; Lee, T.; Seo, E.; Char, K.; Kim, B.-S. *Nanoscale* **2011**, *3*, 4515.
(27) Lee, D. W.; Hong, T. K.; Kang, D.; Lee, J.; Heo, M.; Kim, J. Y.; Kim, B. S.; Shin, H. S. *J. Mater. Chem.* **2011**, *21*, 3438.
(28) Hwang, H.; Joo, P.; Kang, M. S.; Ahn, G.; Han, J. T.; Kim, B.-S.; Cho, J. H. *ACS Nano* **2012**, *6*, 2432.
(29) Eda, G.; Yamaguchi, H.; Voiry, D.; Fujita, T.; Chen, M.; Chhowalla, M. *Nano Lett.* **2011**, *11*, 5111.
(30) King, L. A.; Zhao, W.; Chhowalla, M.; Riley, D. J.; Eda, G. *J. Mater. Chem. A* **2013**, *1*, 8935.
(31) Py, M. A.; Haering, R. R. *Can. J. Phys.* **1983**, *61*, 76.
(32) Lee, C.; Yan, H.; Brus, L. E.; Heinz, T. F.; Hone, J.; Ryu, S. *ACS Nano* **2010**, *4*, 2695.
(33) Li, S.-L.; Miyazaki, H.; Song, H.; Kuramochi, H.; Nakaharai, S.; Tsukagoshi, K. *ACS Nano* **2012**, *6*, 7381.
(34) Li, Y.; Xu, C.-Y.; Hu, P.; Zhen, L. *ACS Nano* **2013**, *7*, 7795.
(35) Chakraborty, B.; Bera, A.; Muthu, D. V. S.; Bhowmick, S.; Waghmare, U. V.; Sood, A. K. *Phys. Rev. B* **2012**, *85*, 161403.
(36) Splendiani, A.; Sun, L.; Zhang, Y.; Li, T.; Kim, J.; Chim, C.-Y.; Galli, G.; Wang, F. *Nano Lett.* **2010**, *10*, 1271.

(37) Lee, J. E.; Ahn, G.; Shim, J.; Lee, Y. S.; Ryu, S. *Nat. Commun.* **2012**, *3*, 1024.
(38) Shi, H.; Yan, R.; Bertolazzi, S.; Brivio, J.; Gao, B.; Kis, A.; Jena, D.; Xing, H. G.; Huang, L. *ACS Nano* **2012**, *7*, 1072.
(39) Huard, V.; Cox, R. T.; Saminadayar, K.; Arnoult, A.; Tatarenko, S. *Phys. Rev. Lett.* **2000**, *84*, 187.
(40) Ross, J. S.; Wu, S.; Yu, H.; Ghimire, N. J.; Jones, A. M.; Aivazian, G.; Yan, J.; Mandrus, D. G.; Xiao, D.; Yao, W.; Xu, X. *Nat. Commun.* **2013**, *4*, 1474.
(41) Peimyoo, N.; Li, J.; Shang, J.; Shen, X.; Qiu, C.; Xie, L.; Huang, W.; Yu, T. *ACS Nano* **2012**, *6*, 8878.
(42) Spivak, B.; Kravchenko, S. V.; Kivelson, S. A.; Gao, X. P. A. *Rev. Mod. Phys.* **2010**, *82*, 1743.
(43) Zhao, W.; Ribeiro, R. M.; Toh, M.; Carvalho, A.; Kloc, C.; Castro Neto, A. H.; Eda, G. *Nano Lett.* **2013**, *13*, 5627.

dx.doi.org/10.1021/nl502883a | *Nano Lett.* XXXX, XXX, XXX−XXX